Biomass Conversion and Biorefinery (2023) 13:3209–3226
https://doi.org/10.1007/s13399-021-01398-w

ORIGINAL ARTICLE

Effect of coconut coir and regenerated silk microparticles as blends and natural binders for construction and demolition waste (CDW) wood on the mechanical, thermal, and structural properties of biomicrocomposites prepared by hot-pressing

Mohammed Abdullah Hamad Alharbi[1] · Shinji Hirai[1] · Toshihiro Kuzuya[1] · Hoang Anh Tuan[2] · Shota Akioka[1]

Received: 26 November 2020 / Revised: 6 February 2021 / Accepted: 22 February 2021 / Published online: 23 March 2021

Abstract

This study aims to utilize the thermosetting behavior of native lignin and the self-assembly of silk in coconut coir (CC) and regenerated silk (RS) microparticles used as blends and natural binders for construction and demolition waste (CDW) wood and their effect on the mechanical, thermal, and structural properties of CDW wood/CC, RS/CC, and CDW wood/RS biomicrocomposites. The obtained biomicrocomposites were prepared by hot-pressing blended microparticles at weight ratios of 80:20, 60:40, 50:50, 40:60, and 20:80 in the temperature range of 170–180°C. The obtained biomicrocomposites were characterized by bending strength, water resistance, scanning electron microscopy (SEM), thermogravimetric analysis/derivative thermogravimetry (TGA/DTG), and attenuated total reflectance Fourier transform infrared spectroscopy (ATR-FTIR) measurements. Findings showed that the incorporation of RS displayed superior enhancement in the mechanical properties and water resistance in CDW/RS. The incorporation of CC slightly improved these properties in CDW/CC and RS/CC but offered greater thermal stability, as shown by thermogravimetric analysis (TGA/DTG). The addition of RS and CC showed good interfacial adhesion, as revealed by SEM. FTIR data revealed strong reactivity among CC, RS, and CDW wood.

Keywords Lignocellulosic biopolymer · Hot-pressing · Microfibrillated biomass waste · Regenerated silk · Lignin binding

1 Introduction

Recently, researchers have focused on the utilization of natural fibers to develop environmentally friendly materials due to environmental issues. Cellulosic biowaste results from construction and demolition waste. Furthermore, recycling fibrous waste generated during crop cultivation and pruning into value-added materials is becoming increasingly popular and economically feasible. For example, high-lignin fibrous waste, such as coir and pith generated from coconut production [1], is attributed to 35% of the total weight of coconut fruit [2], and only 15–20% utilization has been estimated [3]. However, in developing countries, natural fibrous waste has not been utilized efficiently and is processed as waste. Therefore, open burning of agricultural fibrous waste is typically the standard waste management procedure, which causes a major environmental issue due to its contribution to greenhouse emissions [4]. Furthermore, energy production from natural fibers generates fly ash waste and requires intensive chemical pretreatment processes that limit energy production efficiency [5].

CDW wood is used as a filler in wood-plastic composites to increase the biological content and thermal stability of composites [6] but has a poor effect on mechanical properties due to the low reactivity between plastics and wood. Utilization of natural raw fibers as reinforcement materials in composites has been widely reported in the literature [7–11], while others have reported the need for the chemical pretreatment of fibers with/without coupling agents [12–16] by removing lignin and waxes that hinder adhesion in composites and enhance

✉ Mohammed Abdullah Hamad Alharbi
mohammedahalharbi@gmail.com

[1] Research Center of Environmentally Friendly Materials Engineering, Muroran Institute of Technology, 27-1 Mizumoto-cho, Muroran, Hokkaido 050-8585, Japan

[2] Research Institute of Technology for Machinery, Vietnam Engine and Agricultural Machinery Corporation-Joint stock Company, Technology and Alloys of Casting Department, No. 25 Vu Ngoc Phan, Hanoi 100000, Vietnam

adhesion between natural fibers and the matrix. However, many recent studies have focused on the lignocellulose biomass valorization of isolated cellulose or lignin. For example, cellulose is chemically isolated from plant fibers as nanofibers (CNFs) in biocomposite applications [17–19]. Nevertheless, the valorization of lignocellulosic fibrous waste to produce nanofibrillated cellulose requires harsh chemical extraction to extract cellulose from lignin and other materials. Therefore, producing nanofibrillated cellulose might only be environmentally beneficial in natural fibers containing low lignin contents.

On the other hand, technical lignins, a byproduct of chemical extraction, are used as fillers in composites [20] and PLA-lignin biocomposites [21–23]. While the incorporation of technical lignins in small amounts in composites improved the mechanical properties, ultraviolet (UV) light resistance, and thermal stability [24], increasing the content of technical lignin negatively influenced the mechanical properties because it played a role as a filler; hence, chemical modification to enhance reactivity using esterification or grafting is often required [25]. Furthermore, the chemical structure of technical lignins is greatly altered, leading to severe damage to their functionality and impurities that limit their use in value-added products [26–28].

The exploitation of native lignin condensation in natural fibers produces binderless particleboards prepared by hot-pressing, as reported in many studies [29–36]. Furthermore, binderless high-performance particleboards prepared by hot-pressing milled coconut husk fibers/pith without any pretreatment have been reported in Ref. [1]. The findings showed that superior physical properties were attributed to efficiently achieve good lignin condensation due to the microfibrillation—ball milling—of the high-lignin lignocellulose fibers that preserve the lignin chemical structure responsible for its intrinsic thermosetting behavior. In addition, binderless compact wood has also been prepared by steam hot-pressing milled Japanese cedar/cypress wood [37, 38], where 20 wt% (≤53 μm) microparticles were attributed to superior bending strength.

Recently, we reported high-strength lignocellulosic biopolymers (flexural strength of ~122±14 MPa) prepared by hot-pressing microfibrillated raw and alkaline-pretreated palm biomass microparticles (≤53, ≤53–75, and ≤106 μm) [39, 40]. The findings revealed a direct correlation between the chemical composition and particle size of lignocellulosic biomass in achieving optimum lignin binding and their effect on mechanical and thermal properties. Moreover, the higher the ratio of structural materials (cellulose and lignin) to nonstructural materials (hemicellulose, extractives, and ash) (C+L)/(H+E+A) and the smaller the particle size are, the higher the mechanical and thermal properties. This was attributed to the disruption of crystalline regions in cellulose by microfibrillation—ball milling—which exposed more lignin to the surface while preserving its thermosetting behavior, allowing for better adhesion. Furthermore, the mechanical and thermal properties of mildly alkaline-pretreated (1 wt% NaOH, 3 wt% NaOH) plant fibers were improved by removing nonstructural materials without altering the chemical structure of lignin.

Additionally, protein-based biopolymers prepared by thermal processing have been reported in commercial silk microparticles with 20 wt% added water using spark-plasma sintering (SPS) [41], *Bombyx mori* and *Eri* nondegummed silk-based resin was prepared from milled microparticles (~70 μm) [42], regenerated silk-based thermoplastics were prepared from nanoparticles [43], and regenerated silk (sericin free)-based thermoplastics were prepared from hot-pressing followed by the subsequent hot rolling of boiling water-pretreated resins [44]. Findings showed that many factors influencing the binding behavior and mechanical properties of protein-based biopolymers and thermoplastics are attributed to the self-assembly and rearrangement of the molecules of silk in the presence of bound water, which is governed by the amino acid composition (the ratio of hydrophilic to hydrophobic amino acids), size, and orientation of particles.

Lignocellulosic- and silk-based biopolymers prepared by hot-pressing individually exhibited good bending strength and thermal properties. However, incorporating regenerated silk microparticles into PBAT/PLA composites [45] results in poor mechanical properties due to weak adhesion and poor dispersion. Furthermore, cellulose/protein or lignin/protein blends [46–49] are blended using solvent systems such as ionic liquids to dissolve, and then, proteins, cellulose, and lignin are blended to prepare hybrid composites. Nevertheless, this will also destroy an essential feature of native lignin, whose chemical structure is responsible for the thermosetting behavior. When hot-pressing lignocellulosic microparticles, lignin undergoes a glass "thermosetting" transition from 140 to 180°C, which enables the formation of covalent bonds by condensation between lignin and other constituents and interunit linkages and double bonds between lignin units [50–52]. Similarly, amorphous silk nanoparticles and microparticles undergo a structural "thermoplastic" transition during similar hot-pressing conditions, which allows for the formation of more crystalline β-sheet structures [42–44].

Therefore, we hypothesize that utilizing native lignin's ability to bind and self-assemble (thermal fusion phase) silk found in abundant sources, such as coconut coir and regenerated silk, can produce natural binders for use in hybrid biomicrocomposites, resulting in superior mechanical and thermal properties. Furthermore, these natural binders are better than traditional solvent systems, polypropylene (PP), and urea phenol-formaldehyde, which are typically used in lignocellulosic/protein-blended composites, wood-plastic composites, and conventional particleboards, respectively. To the best of our knowledge, no studies have reported utilizing coconut coir and regenerated silk microparticles as green binders of cellulosic waste, such as construction and

demolition waste (CDW) wood or protein/lignocellulosic hybrid biomicrocomposites, at the macroscopic (micrometer) level.

This work reports three types of hybrid biomicrocomposites fabricated by hot-pressing blended microparticles of CDW wood/coconut coir, regenerated silk/coconut coir, and regenerated silk/CDW wood at weight ratios of 80:20, 60:40, 50:50, 40:60, and 20:80. Furthermore, it compares the mass ratio and binding effect of coconut coir- and regenerated silk-based microparticles in terms of mechanical, physical, thermal, and structural properties. The findings of this work can provide insights into the potential of utilizing lignocellulosic and protein fibrous waste as blends or natural binders, replacing the need for petrochemical-based adhesives. Furthermore, there are differences between lignocellulosic- and protein-based binders, and the properties needed for the intended applications can be tailored by manipulating their mass ratio in hybrid biomicrocomposites.

2 Materials and methods

2.1 Materials

Raw coconut coir microparticles (particle size ≤53 μm, moisture content of 9.1%) were obtained by ball milling and then sieving mature coconut coir that was originally harvested in Malaysia and purchased from a commercial supplier. The chemical composition of coconut coir microparticles (46 ± 0.5% α-cellulose, 28 ± 0.5% lignin, 16 ± 0.5% hemicellulose, 10±2% extractives, 2.34% ash) and preparation process were previously described in our work [39]. Construction and demolition waste (CDW) wood powder (mean particle size ≈114 μm, moisture content of 5.97%, ash content of 7.59%) was donated by Air Water ECOROCA Inc. (Japan). Commercially available degummed *B. mori* silk (sericin-free) microparticles (average particle size ≈7 μm, moisture content 8.18%, ash content 0.02%) were purchased from KB Seiren, Ltd. (Japan). The amino acid composition of regenerated silk microparticles (0.53% proline, 42.75% glycine, 10.51% serine, 1.35% glutamine, 1.82% asparagine, 0.11% cysteine, 0.98% threonine, 0.28% lysine, 0.19% histidine, 0.52% arginine, 30.61% alanine, 0.04% methionine, 2.35% valine, 0.76% phenylalanine, 0.68% isoleucine, 0.54% leucine, and 5.68% tyrosine) was reported in Ref. [44].

2.2 Biomicrocomposite preparation

First, 0.9 g of blended microparticles was adjusted to obtain CDW wood/coconut coir, regenerated silk/coconut coir, and regenerated silk/CDW wood at mass ratios of 80:20, 60:40, 50:50, 40:60, and 20:80 and then mixed manually using an agate mortar and pestle. A schematic of sample preparation is presented in Fig. 1. The samples were placed in stainless steel Ø20-mm cylindrical molds and positioned in a hot press (H300-05, AS One, Japan) wherein the top and bottom plates were set at 170°C and wrapped by a heating belt at 180°C used to accelerate heat transfer to the mold. The processing pressure was maintained at 20 MPa, and then, samples were extracted when the optimum temperature reached 170°C for the CDW/CC and CDW/RS wood biomicrocomposites and 180°C for the RS/CC biomicrocomposites. Subsequently, the disc-shaped biomicrocomposite specimens shown in Fig. 2 were gradually cooled at room temperature and dried in a vacuum oven at 100°C between 24 and 48 h to avoid influence of moisture content before testing. The prepared samples, their corresponding labels, and their composition are denoted in Table 1.

2.3 Determination of apparent density

Density was characterized by an analytical balance (AUX120, SHIMADZU, Co., Japan) using Archimedes' principle.

2.4 Bending strength

The three-point bending strength, elastic modulus, and strain at break were evaluated using a tensile tester with a 1 kN maximum loading capacity (Autograph AGS-X, Japan) according to the Japanese standard for testing flexural properties, JIS-K-7171 [53]. Small plate-shaped samples were cut from each sample to obtain 3-mm-wide × 20-mm-long × 2-mm-thick test pieces. The crosshead speed and support span length were set to 1 mm/min and 14 mm, respectively.

2.5 Water absorption and thickness swelling

The water absorption (WA) and thickness swelling (TS) of the samples were calculated according to sections 7.10 and 7.11 of the Japanese industrial standard for water absorption and thickness swelling, JIS-A-5905, respectively [54]. Samples were completely dried to a constant weight in a vacuum oven at 105°C. The samples were then cooled to a constant weight, and sample weight and thickness were measured before the samples were immersed for 24 h in a flask containing 50 mL of distilled water. The immersed samples were wiped with a dry cloth, and water absorption and thickness swelling were determined by weighing the samples and using Eq. 1 and Eq. 2, respectively, as follows:

$$\text{Water absorption}\ (\%) = \frac{(M_2 - M_1)}{(M_1)} \times 100, \quad (1)$$

$$\text{Thickness swelling}\ (\%) = \frac{(T_2 - T_1)}{T_1} \times 100, \quad (2)$$

where M_2 and T_2 are the weight and thickness of the sample

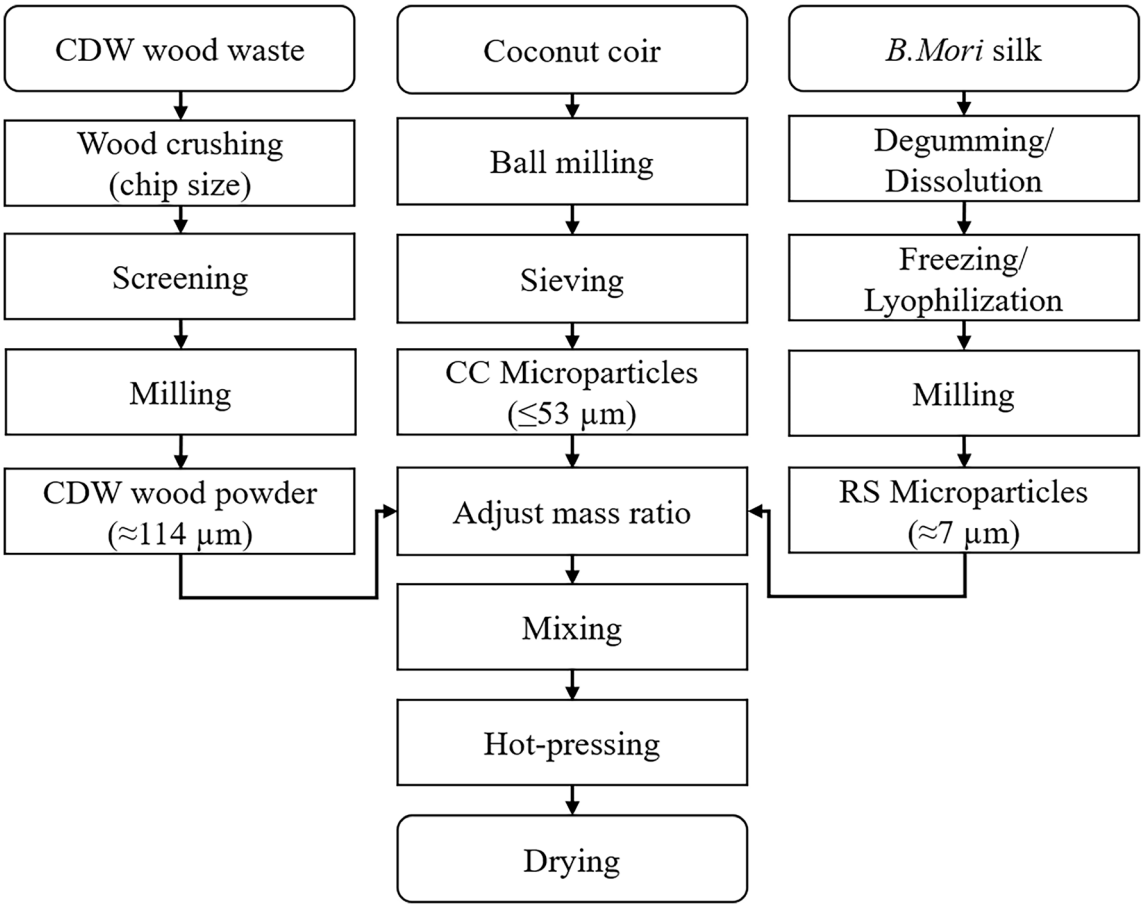

Fig. 1 Flow process diagram of the preparation process of biomicrocomposites

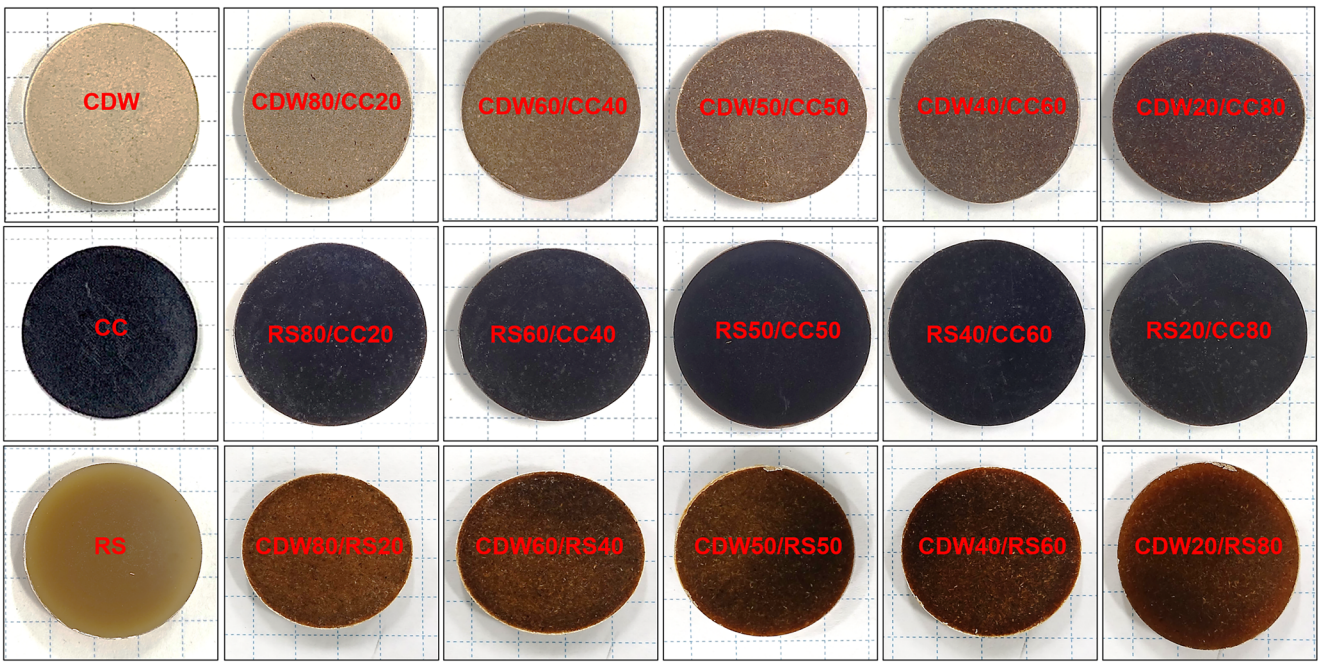

Fig. 2 The appearance of obtained neat biopolymers and their hybrid biomicrocomposites

Table 1 The prepared samples, their labels, and compositions (wt%)

Sample code	Composition (wt%)		
	Coconut coir	CDW wood	Regenerated silk
CC	100	-	-
CDW	-	100	-
RS	-	-	100
CDW80/CC20	20	80	-
CDW60/CC40	40	60	-
CDW50/CC50	50	50	-
CDW40/CC60	60	40	-
CDW20/CC80	80	20	-
CDW80/RS20	-	80	20
CDW60/RS40	-	60	40
CDW50/RS50	-	50	50
CDW40/RS60	-	40	60
CDW20/RS80	-	20	80
RS80/CC20	20	-	80
RS60/CC40	40	-	60
RS50/CC50	50	-	50
RS40/CC60	40	-	60
RS20/CC80	20	-	80

immersed for 24 h, respectively, and M_1 and T_1 are the initial sample mass and thickness, respectively.

2.6 Statistical analysis

The results were statistically analyzed using analysis of variance (ANOVA) carried out by data analysis software (OriginPro, Version 2020b, OriginLab Co., USA) to calculate the mean results (± SE). Mean comparison at the 0.05 level of significance ($\rho \leq 0.05$) was performed according to Tukey's comparison. Three samples or more were used to determine the apparent density, bending strength, water absorption, and thickness swelling.

2.7 Scanning electron microscopy

Scanning electron microscopy (SEM) micrographs captured using a JSM-6510 system (JEOL, Ltd., Japan) were used to investigate the starting material shape and size and compare the morphologies of neat biopolymers and their biomicrocomposites. First, the samples were fixed onto an aluminum tray with conductive tape and coated with a thin layer of carbon fiber using a carbon coating system (Carbon Coating System CC-40F, Meiwafosis, Osaka, Japan). Then, the samples were placed in an SEM chamber, and the starting materials were recorded at ×120 and ×190 magnification, while neat biopolymers and biomicrocomposites at specified mass ratios were captured at ×190 magnification.

2.8 Thermogravimetric analysis/derivative thermogravimetry

Thermogravimetric analysis (TGA) and derivative thermogravimetry (DTG) were performed using a thermogravimetric analyzer (EXSTAR TG/DTA 6300, Seiko Instruments, Inc., Japan) to analyze the thermal behavior of the prepared hybrid biomicrocomposites. Samples weighing 21–30 mg were heated at 10°C/min in the range of 30–700°C in air. The samples were dried in an oven to avoid the influence of moisture content before testing, and measurements were conducted under an oxidative atmosphere to ensure complete decomposition. Mass loss percentage (%) was determined from TGA curves, where the onset temperature (T_{onset}) was defined as the temperature at which 1% mass loss was observed from the TGA curves, and the endset weight (%) was determined at 700°C; the major degradation peaks were identified and selected from the DTG curves. Furthermore, the moisture and ash contents of the starting materials of samples weighing 5–12 mg were obtained from the weight loss (%) measured at 130 and 700°C in accordance with the method reported previously in Ref. [39] and are shown in the supplementary material (Fig. S1, Table. S1).

2.9 Attenuated total reflectance Fourier transform infrared spectroscopy (ATR-FTIR)

FTIR spectra (JASCO FT/IR-6600, JASCO Co., Japan) were generated by performing 45 scans per sample for biomicrocomposites and their corresponding biopolymers using the attenuated total reflectance (ATR) method for wavenumbers in the range of 700–4000 cm^{-1} at 4 cm^{-1} resolution to identify functional groups and the chemical composition based on the functional groups in the "fingerprint" region according to the method described in Ref. [39, 55], which was slightly modified to determine the cellulose, lignin, and hemicellulose contents in CDW/CCs and the β-sheet, cellulose, and hemicellulose contents in RS/CC and CDW/RS biomicrocomposites, as well as in their neat biopolymers. First, the spectra of biomicrocomposites were grouped with their corresponding biopolymers and normalized to values of [0,1]. Second, peaks and peak areas associated with cellulose (A_{895}, A_{1160}, A_{1312}, A_{1370}, and A_{1420}), lignin (A_{1507} and A_{1595}), hemicellulose (A_{1735} and A_{1745}), and β-sheets (A_{1620} and A_{1697}) were identified by second derivative integration from a straight baseline, 20-point adjacent averaging, used as a smoothing method, and 10% threshold height peak filtering in the "fingerprint" region according to specified wavenumber ranges shown in Table 2. The peak area summation associated with cellulose, lignin, hemicellulose, and β-sheets

Table 2 Peak finding ranges associated with the functional groups of cellulose, lignin, hemicellulose, and β-sheet in biocomposites, as determined for the associated peak areas' summation according to the method described in Ref. [39, 55] with slight modification

Assignment	Peak area	Peak range	Ref
β-Glycosidic linkage (amorphous cellulose)	A_{895}	880–915	[56, 57]
C-O-C antisymmetric stretching (cellulose)	A_{1160}*	1140–1185	[55]
CH_2 symmetric bending (cellulose)	A_{1312}	1300–1330	[56, 57]
COH in-plane bending (cellulose)	A_{1370}	1345–1385	[56, 57]
CH_2 symmetric bending (cellulose)	A_{1420}	1400–1440	[57, 58]
C=C aromatic skeletal vibration (lignin)	A_{1507}*	1490–1530	[55, 59]
C=O aromatic skeletal vibration (lignin)	A_{1595}*	1580–1710	[55, 59]
Carbonyl C=O stretching (hemicellulose)	A_{1735}, A_{1745}	1710–1750	[60]
C=O stretching in amide I (β-sheet)	A_{1620}	1616–1622	[61, 62]
C=O stretching in amide I (β-sheet)	A_{1697}	1697–1701	[61, 62]

*Excluded from peak area summation in biomicrocomposites containing regenerated silk due to peak overlapping among regenerated silk secondary structures and cellulose and lignin in plant fibers

was used to note the differences in the chemical compositions of the obtained biomicrocomposites. However, peak areas associated with the C-O-C antisymmetric stretching of cellulose (A_{1160}) and aromatic vibration of phenol groups associated with lignin (A_{1507}, and A_{1591}) excluded peak summations in RS/CC and CDW/RS biomicrocomposites due to either overlapping or combined peaks found in the secondary structure of regenerated silk (amide III, amide II, and amide I).

The results were statistically analyzed using ANOVA to calculate the means and statistical errors (± SE) from two samples for each biopolymer and bio microcomposite. Operations were conducted using graphing and data analysis software (OriginPro, Version 2020b, OriginLab Co., USA).

3 Results and discussion

3.1 Mechanical and physical properties

As shown in Table 3, CC exhibited higher bending strength, Young's modulus, and apparent density than regenerated silk (RS)-based biopolymers, whereas RS exhibited the lowest water absorption (~9 ± 0.43%) and thickness swelling (~7 ± 0.54%) of all other samples. Moreover, CDW reported a similar density as RS but exhibited the lowest bending strength and highest strain at break, Young's modulus, water absorption (~67 ± 3.67%), and thickness swelling (~47 ± 4.33%) among the other samples. Furthermore, CC and RS showed statistically significant differences in the means of bending strength and apparent densities, while all the mechanical and physical properties of CDW were significantly different from those of CC and RS, except the density of RS.

Furthermore, CC has better mechanical and physical properties than CDW, which is attributed to its chemical composition, particularly its higher ratio of cellulose (reinforcing material) and native lignin (binding agent) to hemicellulose, extractives, and ash contents (nonstructural materials). In addition, a smaller microparticle size allows for more lignin trapped between microfibrils to be exposed to the surface, thereby activating efficient lignin binding [39]. On the other hand, the superior mechanical properties of silk-based biopolymers were attributed to the structural transition from a highly random coil/α-helix structure (amorphous structure) to a β-sheet (crystalline structure) by hot-pressing. This structural transition to β-sheets is governed by particle size (microparticles or nanoparticles) and the presence of bound water or water uptake due to the higher

Table 3 Means of the mechanical and physical properties (± SE) of obtained neat biopolymers

Sample	Bending strength (MPa)	Strain at break (%)	Young's modulus (GPa)	Density (g/cm^3)	Water absorption (%)	Thickness swelling (%)
CC	114 ± 1.8^a	1.70 ± 0.06^a	6.42 ± 0.17^a	1.45 ± 0.00^a	12 ± 0.82^a	9 ± 0.85^a
CDW	34 ± 2.3^b	2.73 ± 0.37^b	2.01 ± 0.24^b	1.35 ± 0.01^b	67 ± 3.67^b	47 ± 4.33^b
RS	95 ± 5.2^c	1.57 ± 0.14^a	5.56 ± 0.44^a	1.36 ± 0.01^b	9 ± 0.43^a	7 ± 0.54^a

*Values with different letters in the same column indicate that the difference of means is significant at the 0.05 level ($p \leq 0.05$) among CC, CDW, and RS biopolymers.

ratio of hydrophilic to hydrophobic amino acids [42–44]. Therefore, regenerated silk-based biopolymers reported bending properties equivalent to those of regenerated silk resin in Ref. [44] and slightly lower bending properties than nondegummed *B. mori* silk-based resins (bending strength of 122 MPa) [42] but inferior to those of regenerated silk nanoparticle-based thermoplastics (flexural stress of 160 MPa, flexural strain of 2.5%), as reported in Ref. [43].

As shown in Table 4, incorporating CC exhibited an overall gradual increase in the mechanical and physical properties of CDW/CC biomicrocomposites, exhibiting the best properties at 80 wt% CC (CDW20/CC80). Furthermore, CDW/CC biomicrocomposites at ≤ 40 wt% CC loading showed overall statistically significant differences in mechanical and physical properties, except density. This is because native lignin, which is the binding agent, accounts for only 28 wt% of the chemical composition of coconut coir, as reported in Ref. [39]. Therefore, efficient lignin-based adhesion might be noticeable only in coconut-rich biomicrocomposites due to an increase in the ratio of cellulose and lignin to hemicellulose, extractives, and ash [39]. The gradual increase in the water resistance of CDW/CC biomicrocomposites is also correlated with efficient lignin binding by increasing coconut coir content and decreasing contents of hydrophilic constituents that contain hydroxyl group sites that are reactive with water, such as cellulose [63]. It is possible that, during hot-pressing, efficient wettability of higher lignin content in CDW/CC biomicrocomposites enabling it form covalent bonds by condensation [51], carbon-oxygen (C–O), and carbon-carbon (C–C) bonds through lignin's interunit linkages [52] and intermolecular hydrogen bonds between hydroxyl groups of amorphous regions in cellulose and that aromatic skeletal vibration occur due to the phenol and hydroxyl groups in lignin [63].

Furthermore, RS/CC biomicrocomposites show the highest mechanical properties due to strong adhesion, good dispersion, and compatibility between regenerated silk and lignocellulose after hot-pressing, as shown in Table 5. Furthermore, RS/CC biomicrocomposites inherit the superior properties of their neat biopolymers and show slight differences in mechanical and physical properties according to their mass ratio; however, the water resistance is slightly lower in biomicrocomposites than in neat RS and CC. The mean bending strength, strain, and Young's modulus of RS/CC biomicrocomposites, except for the bending strength of RS20/CC80, show no significant differences from those of RS. Nevertheless, there were significant differences in the densities of the RS/CC biomicrocomposites with coconut coir loading amounts ≤ 50 wt% from those of RS. Additionally, there were statistically significant differences in water absorption and thickness swelling from those RS, but water absorption with a CC loading amount of 20 wt% and thickness swelling with CC loading amounts of 20–40 wt% were not significantly different from those of RS.

On the other hand, Table 6 shows that the mechanical properties of the CDW/RS biomicrocomposites decrease gradually in regenerated silk-rich samples, exhibiting maximum bending strength, strain, and Young's modulus when prepared with 20 wt% regenerated silk (CDW80/RS20). This was also observed for blended films prepared from silk fibroin/cellulose [48] and wool/cellulose [47], where the highest mechanical, physical, and thermal properties were achieved with protein blending (20–25 wt%). CDW/RS biomicrocomposites show statistically significant differences in all mechanical and physical properties from those of CDW. Additional statistical analysis is provided in the supplementary data as a bar chart (Fig. S2), showing significant differences in the mechanical and physical properties of each biomicrocomposite at different mass ratios and their corresponding biopolymers. Although CDW/RS biomicrocomposites show superior water resistance to CDW/CCs, they exhibit adverse effects by showing a slight decrease in the water resistance of the regenerated silk-rich samples, perhaps due to CDW wood having poor dispersion and cracks caused by moisture escaping during drying.

As shown in Tables 4, 5, and 6, adding coconut coir and regenerated silk had a positive effect on the mechanical and

Table 4 Means of the mechanical and physical properties (± SE) of obtained CDW and CC biopolymers and their hybrid biomicrocomposites

Sample	Bending strength (MPa)	Strain at break (%)	Young's modulus (GPa)	Density (g/cm^3)	Water absorption (%)	Thickness swelling (%)
CDW	34 ± 2.3^a	2.73 ± 0.37^a	2.01 ± 0.24^a	1.35 ± 0.01^a	67 ± 3.67^a	47 ± 4.33^a
CDW80/CC20	45 ± 2.0^b	2.24 ± 0.25^a	2.95 ± 0.37^a	1.36 ± 0.01^a	51 ± 3.10^b	40 ± 1.57^a
CDW60/CC40	56 ± 1.6^b	1.79 ± 0.12^b	4.13 ± 0.22^b	1.36 ± 0.01^a	41 ± 1.58^b	31 ± 1.23^b
CDW50/CC50	54 ± 2.6^b	1.39 ± 0.09^b	4.45 ± 0.37^b	1.35 ± 0.01^a	39 ± 3.33^b	27 ± 1.11^b
CDW40/CC60	65 ± 3.0^b	1.60 ± 0.18^b	4.66 ± 0.47^b	1.37 ± 0.01^a	35 ± 0.93^b	23 ± 1.00^b
CDW20/CC80	85 ± 2.8^b	1.28 ± 0.04^b	6.61 ± 0.19^b	1.43 ± 0.01^b	30 ± 1.19^b	19 ± 0.87^b
CC	114 ± 1.8^b	1.70 ± 0.06^b	6.42 ± 0.17^b	1.45 ± 0.00^b	12 ± 0.82^b	9 ± 0.85^b

*Values with the letter (^{b}) in the same column indicate that the difference of means is significant at the 0.05 level ($p \leq 0.05$) from those of CDW.

Table 5 Means of the mechanical and physical properties (± SE) of the obtained RS and CC biopolymers and their hybrid biomicrocomposites

Sample	Bending strength (MPa)	Strain at break (%)	Young's modulus (GPa)	Density (g/cm^3)	Water absorption (%)	Thickness swelling (%)
RS	95 ± 5.2^a	1.57 ± 0.14^a	5.56 ± 0.44^a	1.36 ± 0.01^a	9 ± 0.43^a	7 ± 0.54^a
RS80/CC20	95 ± 1.8^a	1.49 ± 0.03^a	5.98 ± 0.09^a	1.37 ± 0.01^a	13 ± 1.12^a	9 ± 0.44^a
RS60/CC40	104 ± 1.8^a	1.62 ± 0.04^a	5.91 ± 0.21^a	1.39 ± 0.01^a	15 ± 0.59^b	10 ± 0.98^a
RS50/CC50	105 ± 2.3^a	1.54 ± 0.04^a	6.33 ± 0.14^a	1.39 ± 0.01^b	16 ± 0.95^b	11 ± 0.47^b
RS40/CC60	104 ± 1.5^a	1.61 ± 0.02^a	5.95 ± 0.14^a	1.41 ± 0.01^b	16 ± 1.22^b	12 ± 0.78^b
RS20/CC80	109 ± 3.1^b	1.79 ± 0.04^a	5.65 ± 0.13^a	1.42 ± 0.01^b	18 ± 0.79^b	12 ± 1.42^b
CC	114 ± 1.8^b	1.70 ± 0.06^a	6.42 ± 0.17^a	1.45 ± 0.00^b	12 ± 0.82^a	9 ± 0.85^a

*Values with the letter (^{b}) in the same column indicate that the difference of means is significant at the 0.05 level ($p \leq 0.05$) from those of RS.

physical properties of the CDW/CC and CDW/RS biomicrocomposites. Additionally, RS/CC blends reported higher mean bending strengths, strains, and Young's moduli than the CDW/CC and CDW/RS biomicrocomposites.

RS/CC biomicrocomposites showed an overall better water resistance than CDW/RS biomicrocomposites. Generally, the water resistance of the obtained biomicrocomposites is attributed to the type of adhesion and its efficiency. Therefore, both β-sheet-enriched crystalline and activated lignin-based adhesion were attributed to the better water resistance in RS/CC biomicrocomposites than lignin-based adhesion in CDW/CC or silk-based adhesion in CDW/RS. The obtained CDW/RS and RS/CC biomicrocomposites showed water resistance comparable to that of previously reported raw and alkaline-pretreated coconut coir-based biopolymers. In contrast, all biomicrocomposites showed better water resistance than raw and alkaline-pretreated date fiber- and leaf-based biopolymers [39] and binderless particleboards reported in the literature [31, 64–67]. These findings suggest that incorporating coconut coir- and regenerated silk-based materials as binders or blends positively influences water resistance when used in biomicrocomposites.

Utilizing coconut coir as a natural binder is highly dependent on more native lignin (chemically unaltered) and its efficient binding, while regenerated silk is highly dependent on its ability to form more crystalline-enriched β-sheets from amorphous microparticles. Regenerated silk-based microparticles showed more significant binding for CDW wood because they solely function as a binding agent, unlike 28 wt% of coconut coir-based microparticles. Therefore, it is highly possible that cross-linking occurs among CDW wood, coconut coir, and regenerated silk microparticles during hot-pressing via hydroxyl groups, lignin interunit linkages, lignin phenol groups, and the secondary structure of protein (explained in detail in Section 3.4).

These results suggest that coconut coir- and regenerated silk-based microparticles are suitable candidates for use as natural binders for cellulosic waste, such as CDW wood or as protein/lignocellulose blends. Additionally, the influence of the particle size of CDW wood and coconut coir on the mechanical properties of CDW/CC and RS/CC biomicrocomposites was validated in the supplementary data (Table S2–S3), where biomicrocomposites prepared from smaller particles achieved better mechanical properties than those prepared from larger particles. In addition, Table S4 shows the positive effect of blending raw and mildly alkaline-pretreated bagasse- and coconut coir-based microparticles on the mechanical properties of lignocellulosic

Table 6 Means of the mechanical and physical properties (± SE) of obtained CDW and RS biopolymers and their hybrid biomicrocomposites

Biopolymer	Bending strength (MPa)	Strain at break (%)	Young's modulus (GPa)	Density (g/cm^3)	Water absorption (%)	Thickness swelling (%)
CDW	34 ± 2.3^a	2.73 ± 0.37^a	2.01 ± 0.24^a	1.35 ± 0.01^a	67 ± 3.67^a	47 ± 4.33^a
CDW80/RS20	93 ± 2.6^b	1.81 ± 0.08^b	5.34 ± 0.31^b	1.39 ± 0.00^b	17 ± 1.52^b	12 ± 1.16^b
CDW60/RS40	90 ± 1.4^b	1.50 ± 0.07^b	6.55 ± 0.25^b	1.39 ± 0.00^b	16 ± 0.65^b	13 ± 1.00^b
CDW50/RS50	83 ± 2.9^b	1.42 ± 0.05^b	6.02 ± 0.29^b	1.38 ± 0.00^b	14 ± 1.47^b	12 ± 0.54^b
CDW40/RS60	69 ± 2.4^b	1.18 ± 0.03^b	6.19 ± 0.25^b	1.38 ± 0.00^b	24 ± 1.18^b	13 ± 0.85^b
CDW20/RS80	62 ± 3.6^b	1.08 ± 0.04^b	6.38 ± 0.13^b	1.38 ± 0.00^b	21 ± 1.06^b	12 ± 0.55^b
RS	95 ± 5.2^b	1.57 ± 0.14^b	5.56 ± 0.44^b	1.36 ± 0.01^a	9 ± 0.43^b	7 ± 0.54^b

*Values with the letter (^{b}) in the same column indicate that the difference of means is significant at the 0.05 level ($p \leq 0.05$) from those of CDW.

biomicrocomposites, regardless of the mass ratio, and better mechanical properties than blends of CDW wood- or untreated lignocellulosic-based microparticles were achieved. These results suggest that raw high-lignin or mildly alkaline pretreated plant fiber sources such as coconut coir or bagasse are suitable candidates for fabricating high-performance biomicrocomposites or serving as binders for CDW wood. These findings may be evidence that suggests a potential shift from synthetic binder-based adhesion in WPC composites and particle boards to native lignin- or protein-based adhesion, which does not lead to a degradation in mechanical properties. For example, incorporating 10–30 wt% silk fibroin microparticles in PBAT/polylactide PLA blends, as performed in ref. [45], exhibited no change or decrease in flexural strength (38–32 MPa) compared to that of neat PBAT/polylactide PLA blends (39–42 MPa). In addition, mixing microparticles using melt blending by hot-pressing does not require the use of the chemicals used in extraction or solvent systems for "solution blending," such as technical lignins [23, 68].

3.2 SEM morphologies

SEM micrographs of the starting materials exhibited in Fig. 3 confirm the particle size, shape, and orientation of the starting materials, thereby helping explain the adhesion behavior of the obtained biopolymers and biomicrocomposites. Regenerated silk microparticles show uniform and smaller microparticles, while the coconut coir microparticles are irregular and slightly larger and exhibit microfibers. On the other hand, the SEM micrographs of the CDW wood exhibited larger fibers and signs of degradation caused during the processing of CDW waste.

Biopolymers and their corresponding hybrid biomicrocomposite microstructures were observed at ×190 magnification (Fig. 4) and ×120 magnification (Fig. S3). As shown in the SEM micrographs (Fig. 4), CC and RS both showed denser microstructures and smoother surfaces than CDW, which was attributed to the thermosetting behavior of lignin and the self-assembly of regenerated silk, respectively. The morphologies of coconut coir-based biopolymers, hot-pressed CDW wood, and regenerated silk-based biopolymers were examined in Ref. [39, 42], where lignin condensation and β-sheet-enriched crystalline transitional phases were attributed to binding. Although CC and RS morphologies differ due to their binding behavior and microparticle size, CC exhibits a slightly rougher morphology than RS, possibly due to nonstructural materials and cellulose nanofibers in addition to lignin and their random distribution. RS shows a homogenous microstructure, which is attributed to its smaller particle size and structural transition from an amorphous structure to a β-sheet-enriched crystalline structure. On the other hand, the lack of a binding agent and the presence of microfibrils in hot-pressed CDW wood resulted in porous structures and cavities.

Furthermore, SEM micrographs (Fig. 4) illustrated phase separation and composition differences in the obtained biomicrocomposites. Moreover, the incorporation of 50 and 80 wt% coconut coir microparticles in CDW50/CC50 and CDW20/CC80 caused changes in the characteristics and a better morphology than that of CDW. Although more debonding areas and fiber pulling were still visible in CDW50/CC50, CDW20/CC80 showed dense lignin adhesion similar to that in CC. These micrographs confirm that coconut coir-based microparticles functioned as a binder for CDW by increasing the native lignin content, thereby inducing more lignin-based adhesion. On the other hand, regenerated silk/coconut coir blends at mass ratios of 50:50 and 20:80 exhibited morphologies comparable to those of RS and CC, respectively. RS50/CC50 revealed a microstructure including both lignin- and silk-based binding, whereas RS20/CC80 displayed more lignin-based adhesion than CC. This confirms that protein- and lignocellulosic-based microparticles efficiently blend as macromolecules in the RS/CC biomicrocomposites. The thermosetting behavior of lignin and self-assembly of silk phases probably operated as a natural solvent system during hot-pressing, which allowed further distribution of silk and coconut coir microparticles and sufficient integration in RS/CC biomicrocomposites.

In addition, CDW50/RS50 and CDW20/RS80 highlighted the ability of regenerated silk to efficiently function as a binder for CDW wood at much lower contents than coconut coir-based microparticles. The CDW/RS biomicrocomposites with 50 and 80 wt% regenerated silk microparticles displayed a better morphology than CDW50/CC50 and CDW20/CC80, respectively, due to silk-based adhesion. This is due to the transitional phase-based adhesion of regenerated silk, which is attributed to its smaller particle size and absence of impurities, while coconut coir's lignin-based adhesion (accounting for 28 wt%) is attributed to the larger particle size and presence of cellulose and other constituents. As shown in Fig. 5, the effect of adding 20, 40, and 60 wt% regenerated silk to the CDW/RS biomicrocomposites suggests that regenerated silk microparticles are very effective at lower mass ratios since they act as the sole binder rather than the coconut coir. However, CDW20/RS80 with the higher content of regenerated silk microparticles showed cracks and nanosized pores caused by CDW wood agglomeration and their uneven distribution, moisture escape, and thermal degradation during drying.

3.3 Thermal behavior and stability

As shown in Table 7 and Fig. 6, the thermal behavior of the obtained biomicrocomposites was determined by the type of added/blended starting materials and their mass ratio

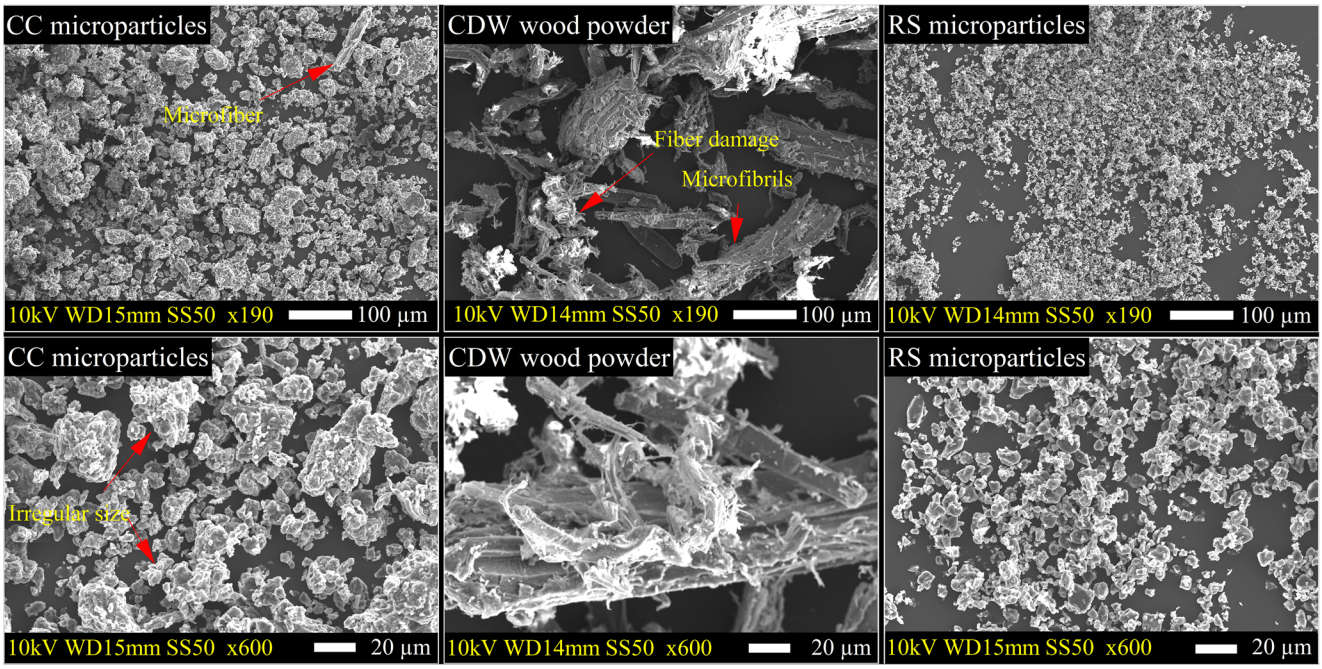

Fig. 3 SEM micrographs of coconut coir microparticles, CDW wood powder, and regenerated silk microparticles captured at ×190 and ×600 magnification, showing particle size and distribution

according to weight loss curves and decomposition peaks obtained by TGA and DTG. Figure 6 a–c shows that RS and CC exhibited similar onset temperatures (at 1% weight loss) in the range of 224–226°C. The high thermal stability of CC is due to the microfibrillation and chemical composition of high-lignin coconut coir, which allows for a more complex and thermally stable form of lignin, thereby resulting in efficient lignin binding [39, 69], while the thermal stability of RS is attributed to the formation of more crystalline β-sheets [43]. On the other hand, hot-pressed CDW reported a lower onset temperature (~190°C) than the other samples. Therefore, CDW/CC biomicrocomposites show an increase in the onset temperature (200–225°C) compared to that of CDW wood. On the other hand, a slight increase in onset temperatures by incorporating only 50 and 60 wt% regenerated silk microparticles was exhibited in CDW50/RS50 and CDW40/RS60 (193–196°C) compared to that of CDW wood. RS/CC biomicrocomposites except for RS80/CC20 show similar or slightly lower onset temperatures (218–221°C) than CC. This suggests that increasing the content of coconut coir microparticles in CDW/CC and RS/CC enhanced thermal stability and showed similar trends in their bending strength and water resistance. Although RS, CDW20/RS80, and RS80/CC20 exhibited high onset temperatures (190–233°C), the remaining residues cannot be determined because extreme vibration caused thermal instability above ~285° in regenerated silk, as shown in the supplementary data (Fig. S4). The CDW/CC biomicrocomposites showed higher endset weight percentage residues (~1.84–3.17%) than the RS/CC biomicrocomposites (1.22–2.44%), while the lowest endset weight percentages were only reported in CDW80/RS20 and CDW60/RS40 at 0.68 and 0.63%, respectively. In addition, the higher endset weights observed in coconut coir- and CDW wood-rich samples were attributed to the ash content in their starting materials being higher than that of regenerated silk (Fig. S1, Table S1).

The DTG curves in Fig. 6d–f show thermal decomposition peaks, thereby explaining the thermal stability of biomicrocomposites. The presence of small sharp peaks in the range of 200–250°C was possibly attributed to the release of nonfrozen bound water and aliphatic OH groups or the decarboxylation of acids in lignin [63, 69, 70]. Similarly, these peaks were also observed in strong lignin adhesion-based lignocellulose biopolymers [39, 40] and regenerated silk thermoplastics [43]. The absence of these peaks in CDW, CDW/CC biomicrocomposites, and CDW80/RS20 may indicate lower contents of condensed lignin and silk. In addition, Fig. 6d shows the DTG curve of CC, exhibiting two decomposition peaks at 260 and 320°C attributed to hemicellulose and cellulose, respectively [60], while condensed lignin decomposes over a broader peak at 280–560°C [52, 71]. CDW wood, on the other hand, shows overlapping hemicellulose and cellulose decomposition peaks and exhibited maximum DTG decomposition at 300°C, suggesting poor thermal stability similar to that of milled plant fibers (Fig. S1, Table S1) and nonlignin-based adhesion biopolymers [39, 40], where condensed lignin has higher thermal stability than in the absence of lignin or less condensed lignin [71]. Therefore, CDW/CC biomicrocomposites exhibited decreased maximum DTG decomposition peaks due to enhanced thermal stability achieved

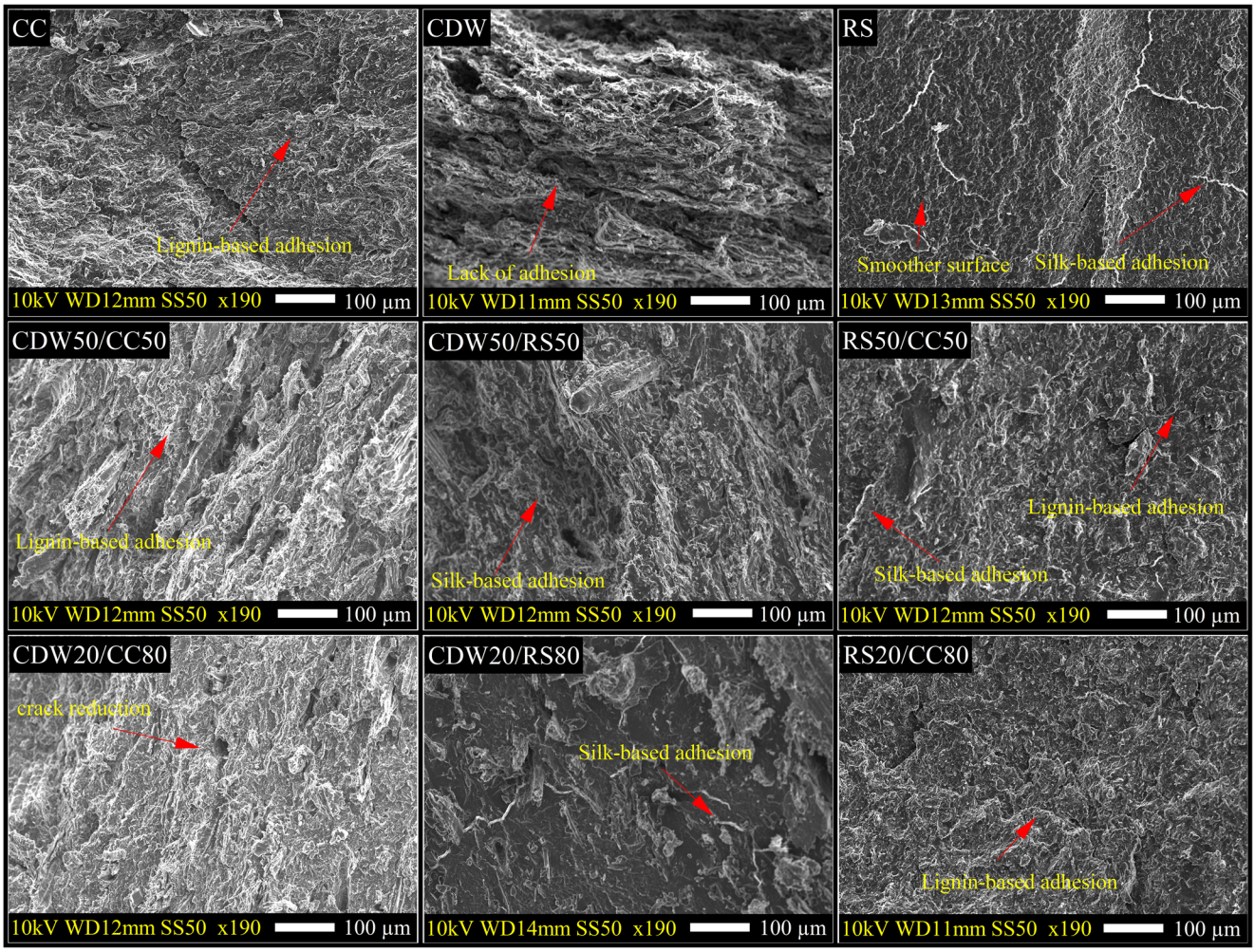

Fig. 4 SEM micrographs of neat biopolymers and their hybrid biomicrocomposites at ×190 magnification

by incorporating more coconut coir-based microparticles due to cellulose and activated lignin, improving thermal stability. Thus, CDW40/CC60 and CDW20/CC80 showed hemicellulose and cellulose decomposition peaks in the ranges of 253–266°C and 300–345°C, respectively. Furthermore, Fig. 6e illustrates the superior thermal stability of RS/CC biomicrocomposites containing CC (40–80 wt%) to CDW/RS containing RS (20–60 wt%); however, RS, RS80/CC20, and CDW20/RS80 were extremely unstable above 285°C, as shown in the supplementary data (Fig. S6). These findings confirm that condensed lignin and cellulose provide good thermal stability around 285°C in RS/CC and CDW/RS, while regenerated silk provides enhanced thermal properties at approximately 300–350°C. Moreover, DTG peaks are exhibited in the range of 400–600°C, and their fluctuations are attributed to char formation [72] and the combustion of biomicrocomposites under an oxidative atmosphere [39, 40, 73]. Overall, CC/RS biomicrocomposites showed superior

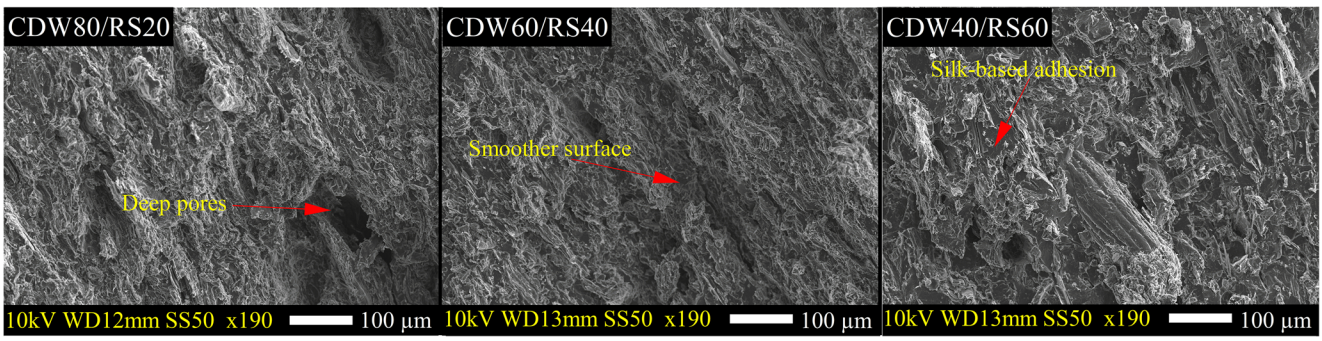

Fig. 5 SEM micrographs showing the effect of adding 20, 40, and 60 wt% regenerated silk to the CDW/RS biomicrocomposites

Table 7 Thermal properties of biocomposites and their corresponding biopolymers

Sample	Onset temperature at 1% (°C)	Maximum degradation peaks (°C)			Endset residues (%)
		i	ii	ii	
CC	224	248	302	542	5.40
CDW	190	-	312	385	2.82
RS*	226	285	-	-	-
CDW80/CC20	213	-	300	410	2.4
CDW60/CC40	200	-	303	416	1.84
CDW50/CC50	211	-	297	455	2.49
CDW40/CC60	215	266	293	450	3.17
CDW20/CC80	225	253	275	505	3.05
RS80/CC20*	233	284	-	-	-
RS60/CC40	223	269	306	544	1.66
RS50/CC50	221	275	306	524	1.22
RS40/CC60	219	256	304	513	1.85
RS20/CC80	218	253	281	514	2.44
CDW80/RS20	183	-	340	563	0.68
CDW60/RS40	186	297	342	581	0.63
CDW50/RS50	193	298	344	584	-
CDW40/RS60	196	298	345	598	-
CDW20/RS80*	190	-	-	-	-

*Thermal behavior cannot be determined due to regenerated silk's thermal instability above 285°C

thermal properties to CDW/CC and CDW/RS biomicrocomposites. Although CDW/RS shows better thermal resistance than CDW/CC, note that a higher regenerated silk content (~80 wt%) causes thermal instability. In addition, comparable enhancement in the thermal resistance of CDW/CC biomicrocomposites was only observed when the coconut coir content is ≥60 wt% due to native lignin's content being responsible for higher stability and accounting for 28 wt% in coconut coir.

3.4 FT-IR spectroscopy

FT-IR spectra were generated for the "fingerprint" and "single bond" regions of hybrid biomicrocomposites and their neat biopolymers, as shown in Fig. 7. Figure 7 a shows small differences in the spectra of the CDW/CC biomicrocomposites, CC, and CDW wood. However, higher mass ratios of CC in CDW/CC biomicrocomposites show a gradual increase in the intensities of the peaks associated with the β-glycosidic linkage of amorphous cellulose at 895 cm^{-1} [56, 57], the C=O stretching of the guaiacyl ring at 1239–1290 cm^{-1} [55], the aromatic skeletal vibrations of the phenol groups of the aromatic ring in lignin at approximately 1594 cm^{-1} [55], and the carbonyl C=O stretching of hemicellulose at 1730–1745 cm^{-1} [60].

On the other hand, Fig. 7 b and c show that the peaks attributed to the lignocellulose-, cellulose-, and protein-based functional groups overlap for the RS/CC and CDW/RS hybrid biomicrocomposites and are assigned as follows: C-O-C antisymmetric stretching of cellulose (1140–1185 cm^{-1}) [74]; the C-C, C-O, and C=O stretching of the G band due to condensation > etherification and the C-N stretching of the amide III band (random coil) (1220–1249 cm^{-1}) [55, 62]; the C=O aromatic skeletal vibrations of phenol groups in lignin (G>S) and the amide II band (N–H) attributed to the bending of β-sheets and random coils in the region (1490–1570 cm^{-1}) [55, 59, 75]; the C=O aromatic skeletal vibrations of phenol groups in lignin (S>G) and the amide I band (C=O) stretching of silk's β-sheet region (1580–1720 cm^{-1}) [55, 61, 62]; C-H_2 symmetric stretching, C-H_3 antisymmetric stretching of lignocellulose, and C-H_2 asymmetric stretching of the amide B band of silk (2700–3000 cm^{-1}) [59, 76]; and O-H stretching of lignocellulose and O-H and N-H stretching of the amide A band of silk (3100–3600 cm^{-1})[59, 76].

By comparing the spectra of RS/CC and CDW/RS biomicrocomposites (Fig. 7b, c), significant differences in peak absorption can be observed, which is directly related to the type and composition of added/blended starting materials. Therefore, the composition of regenerated silk and coconut coir in RS/CC and CDW wood and regenerated silk in CDW/RS biomicrocomposites can be observed from FTIR

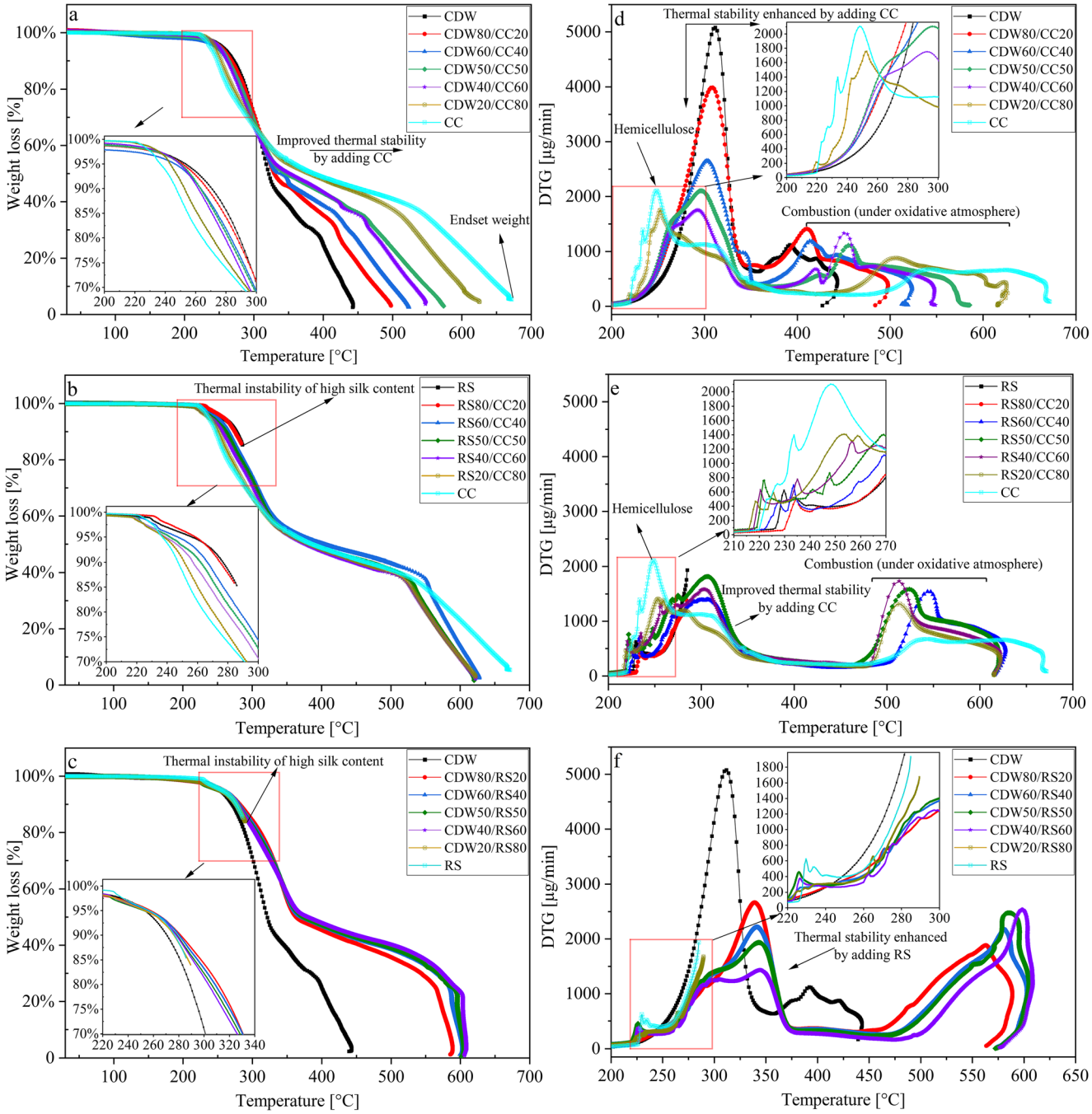

Fig. 6 Mass-loss percentage of **a** CDW and CDW/CC, **b** RS and RS/CC, and **c** CDW/RS biomicrocomposites. Corresponding DTG curves of **d** CDW and CDW/CC, **e** RS and RS/CC, and **f** CDW/RS biomicrocomposites

spectra (Fig. 7b, c), which mimic the FTIR spectra of their corresponding neat biopolymers. For example, silk-rich biomicrocomposites showed an increase in the heights of the peaks at 1230 cm^{-1} attributed to C-N stretching of amide III (Random coil), 1520 and 1620 cm^{-1} attributed to N-H deformation of amide II and I (β-sheet), and in the range 3250–3400 cm^{-1} attributed to the O-H and N-H stretching of amide A. On the other hand, coir- and CDW wood-rich biomicrocomposites exhibited sharp peak at 1023 cm^{-1} attributed to aromatic C-H deformation in guaiacyl and C-O stretching in primary alcohol, which is typically found in plant fibers [55, 57].

The results in Table 8 show an increase in the peak areas associated with cellulose, lignin, and hemicellulose in CDW/CC biomicrocomposites compared to those observed in neat hot-pressed CDW wood. This was attributed to coconut coir

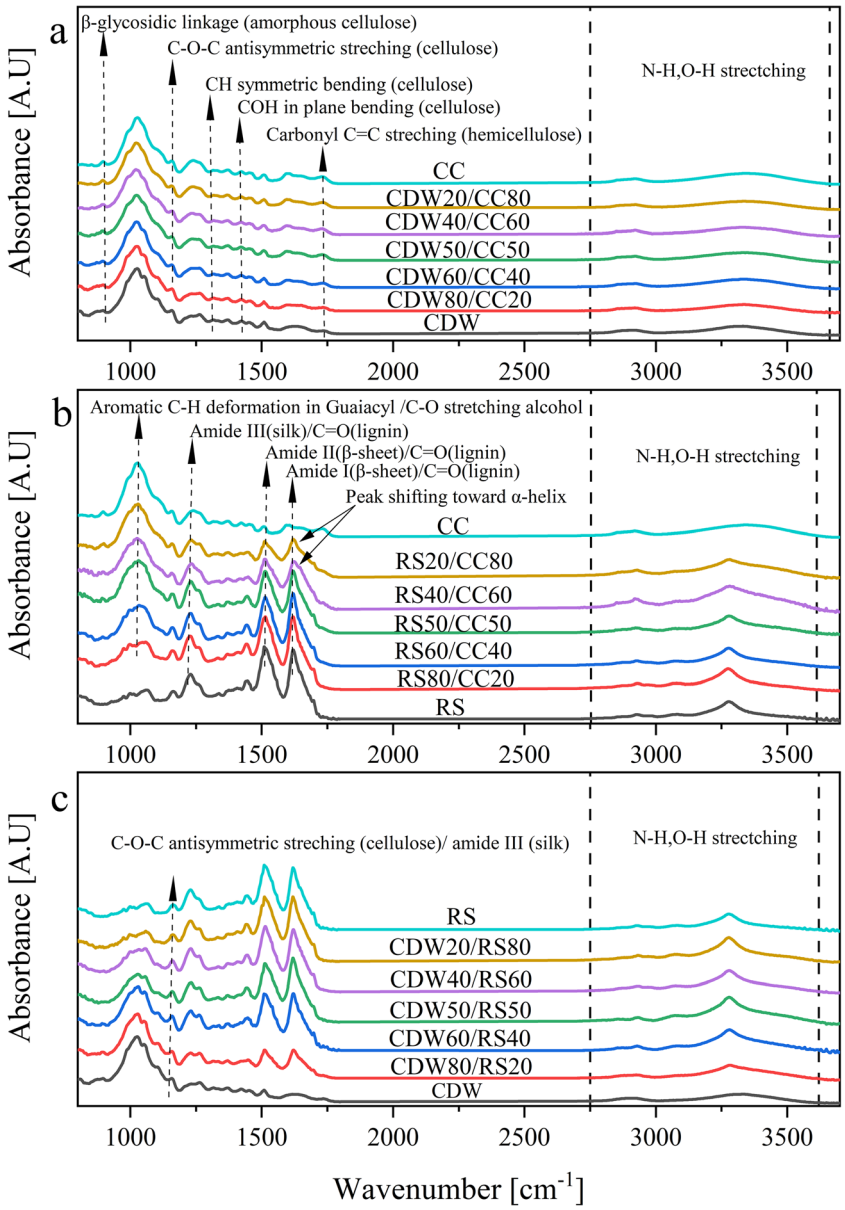

Fig. 7 FT-IR spectra of **a** CDW/CC, **b** RS/CC, and **c** CDW/RS biomicrocomposites and their corresponding biopolymers

loading, which causes composition changes due to the presence of lignin and hemicellulose; CC reported higher summations of peak areas associated with cellulose, lignin, and hemicellulose than hot-pressed CDW wood. Therefore, CDW/CC coconut coir-rich samples reported a higher summation of peak areas associated with lignin and hemicellulose than hot-pressed CDW wood. In addition, the CDW40/CC60 and CDW20/CC80 biomicrocomposites only show a noticeable increase in the summation of peak areas associated with cellulose content compared with that of hot-pressed CDW wood. The higher increase in peak areas based on functional groups associated with lignin agrees with our previous findings for palm fiber- and leaf-based lignocellulosic biopolymers [38], indicating that a higher native lignin content is attributed to binding and thus superior mechanical and thermal properties.

Moreover, the results exhibited in Table 9 describe the peak area summation associated with the functional groups of β-sheets, cellulose, and hemicellulose, which confirm and provide an estimation of composition changes in RS/CC and CDW/RS biomicrocomposites. Moreover, gradual loading of CC and CDW content (≥50 wt%) shows a decrease in the summation of the peak areas associated with β-sheets in RS/CC and CDW/RS biomicrocomposites compared to that in RS. Similarly, a steady rise in cellulose content was observed in the RS/CC and CDW/RS biomicrocomposites containing CC (≥20 wt%) and CDW (≥20 wt%). Additionally, smaller traces of hemicellulose were observed from the summation of the peak areas associated with its functional groups in RS40/CC60, RS20/CC80, and CDW80/RS20.

Table 8 Summation of the major peak areas in the "fingerprint" region associated with cellulose, lignin, and hemicellulose in CDW/CC biomicrocomposites

Sample	∑A(cellulose)[a]	∑A(lignin)[b]	∑A(hemicellulose)[c]
CDW	3.37 ± 0.04	1.62 ± 0.07	0.27 ± 0.05
CDW80/CC20	3.02 ± 0.04	2.24 ± 0.11	0.30 ± 0.03
CDW60/CC40	3.34 ± 0.07	2.37 ± 0.03	0.42 ± 0.07
CDW50/CC50	3.15 ± 0.05	2.45 ± 0.08	0.57 ± 0.02
CDW40/CC60	3.53 ± 0.42	3.04 ± 0.75	0.65 ± 0.07
CDW20/CC80	3.48 ± 0.11	2.72 ± 0.05	0.54 ± 0.01
CC	3.80 ± 0.10	3.35 ± 0.32	0.63 ± 0.13

[a] $\sum A$ (cellulose) = (A_{895}+ A_{1159}+A_{1317}+A_{1370}+ A_{1420})

[b] $\sum A$ (lignin) = (A_{1509} + A_{1592})

[c] $\sum A$ (hemicellulose) = (A_{1735}+A_{1745})

Based on these results, the numerically estimated cellulose and hemicellulose contents confirm the composition of CC and CDW in CC/RS and CDW/RS hybrid biomicrocomposites, respectively. On the other hand, determining the lignin content in RS/CC biomicrocomposites was immensely challenging using this method; however, it can be assumed that the reduction in the β-sheet peak areas was caused by greater or more lignin-based adhesion. Two suggestions can be made from this trend: either lignin peaks overlapped in the amide I and amide II bands of the secondary protein structure or there were strong interactions among the functional groups associated with native lignin, amide I and II, which made it challenging to distinguish lignin's functional groups from others. The latter is highly probable, as indicated by the significant decrease in the summation of the peak areas associated with β-sheets, which was exhibited only in RS40/CC60, RS20/CC80 (Fig. 7b), and CDW80/RS20 (Fig. 7c) when the CC and CDW wood loading amounts were ≥60 wt% and ~80 wt%, respectively. This is considered high compared to that in the technical lignins reported in [77], which showed conformational changes toward a "disordered" phase in thermoplastic zein/lignin bionanocomposites as little as 5 wt% loading of technical lignin. However, we only observed an increase in peak area associated with α-helices in RS40/CC60 and RS20/CC80 and a decreased peak area associated with β-sheets in CDW80/RS20. This arrangement only indicated favorable hydrogen bonding between the functional groups of lignin and α-helices [77], possibly caused by more lignin-based adhesion, rather than a conformational change toward a "disordered" phase. The conformational changes of the secondary protein structure by thermomolding reveals that wavenumbers and peak areas shift according to the conformation of β-sheets, α-helices, and β-turns [77], where higher-intensity peaks of β-sheets and α-helices imply that a more "ordered" phase exists in the secondary structure of proteins, while higher-intensity peaks of β-turns indicate that a "disordered" phase exists in the presence of additives [78]. However, RS/CC and CDW/RS biomicrocomposites showed that conformation toward the formation of β-sheets, attributed to the peak at approximately 1620 cm^{-1}, was unhindered. In addition, possible hydrogen bonding interactions among hydroxyl groups of silk cellulose and lignin were attributed to peaks at approximately 3300 cm^{-1}, a similarly to what observed in cellulose and wool blended films [47].

Table 9 Summation of major peak areas in the "fingerprint" region associated with β-sheets, cellulose, and hemicellulose in biomicrocomposites containing regenerated silk

Sample	∑A(β-sheet)[a]	∑A(cellulose)[b]	∑A(hemicellulose)[c]
RS	30 ± 0.1	-	-
RS80/CC20	32 ± 1.0	0.41 ± 0.00	-
RS60/CC40	31 ± 1.2	0.72 ± 0.01	-
RS50/CC50	26 ± 0.4	0.94 ± 0.18	-
RS40/CC60	18 ± 2.9	0.96 ± 0.06	0.04 ± 0.02
RS20/CC80	12 ± 2.3	1.23 ± 0.24	0.15 ± 0.02
CDW80/RS20	14 ± 1.4	1.41 ± 0.01	0.02 ± 0.02
CDW60/RS40	27 ± 0.6	1.08 ± 0.18	-
CDW50/RS50	33 ± 0.6	0.60 ± 0.10	-
CDW40/RS60	29 ± 1.2	0.42 ± 0.13	-
CDW20/RS80	33 ± 0.4	0.15 ± 0.01	-
CC	-	2.32 ± 0.01	0.62 ± 0.12
CDW	-	2.19 ± 0.00	0.29 ± 0.04

[a] $\sum A$ (β-sheet) = (A_{1620} + A_{1697})

[b] $\sum A$ (cellulose) = (A_{895}+ A_{1317}+A_{1370}+ A_{1420})

[c] $\sum A$ (hemicellulose) = (A_{1735}+A_{1745})

Further evidence indicates that the materials resulting from blending and hot-pressing native lignin in coconut coir and regenerated silk microparticles act as macromonomers instead of additives in biomicrocomposites.

4 Conclusions

Coconut coir- and regenerated silk-based microparticles act as multifunctional natural binders for CDW wood or blends used to prepare hybrid biomicrocomposites. CDW, CC, and RS microparticles were mixed at specified mass ratios and then hot-pressed in the range of 170–180°C. Coconut coir and regenerated silk acted as binders for CDW wood, and regenerated silk/coconut coir blends acted as macromolecules rather than additives in their

respective biomicrocomposites. The binding effect of the incorporation of RS (20–40 wt%) displayed superior enhancement in the mechanical properties and water resistance of CDW/RS. On the other hand, the incorporation of CC slightly improved the mechanical properties and water resistance of CDW/CC and RS/CC but offered greater thermal stability, as shown by thermogravimetric analysis (TGA/DTG). SEM micrographs show that good interfacial adhesion is achieved by blending CC and RS or adding them to CDW wood. FTIR data confirm the compositions and suggest stronger reactivity among cellulose, lignin, and the secondary structure of the protein.

The findings of this work not only suggest the use of natural fiber-based microparticles in biocomposites to enhance the mechanical and thermal properties and biological content but also offer insight into utilizing lignin's and protein's transitional phases as solvent systems during hot-pressing. This can be an alternative to conventional blending methods, such as using ionic liquids to dissolve protein and lignocellulose to prepare hybrid biocomposites. Although native lignin cannot be chemically isolated without disrupting its thermosetting behavior, it will have more multifunctional properties, as reported for technical lignin UV resistance and thermal stability. Furthermore, regenerated silk can be isolated chemically from various silk sources but remains thermoplastic, which could mean that silk/lignocellulose blends could be recyclable.

Supplementary Information The online version contains supplementary material available at https://doi.org/10.1007/s13399-021-01398-w.

Author contribution Mohammed A.H Alharbi: writing (original draft), conceptualization, methodology, formal analysis, investigation, resources, data curation, visualization, and project administration. Shinji Hirai: supervision and writing (review and editing); conceptualization. Toshihiro Kuzuya: supervision and writing (review and editing); conceptualization. Hoang Anh Tuan: validation. Shota Akioka: validation.

Data availability The raw, processed, and filtered data required to reproduce these findings are available to download from https://doi.org/10.17632/dw9mrddpbf.1.

Declarations

Competing interests The authors declare no competing interests.

References

1. Van Dam JEG, Van Den Oever MJA, Teunissen W et al (2004) Process for production of high density / high performance binderless boards from whole coconut husk Part 1 : Lignin as intrinsic thermosetting binder resin. Ind Crop Prod 19:207–216. https://doi.org/10.1016/j.indcrop.2003.10.003
2. Thampan PK (1991) Handbook on Coconut Palm. Oxford and IBH Publishing Co., New Delhi
3. Dam JEG, Van Den Oever MJA, Keijsers ERP (2004) Production process for high density high performance binderless boards from whole coconut husk. Ind Crop Prod 20:97–101. https://doi.org/10.1016/j.indcrop.2003.12.017
4. Wang J, Xi F, Liu Z, Bing L, Alsaedi A, Hayat T, Ahmad B, Guan D (2018) The spatiotemporal features of greenhouse gases emissions from biomass burning in China from 2000 to 2012. J Clean Prod 181:801–808. https://doi.org/10.1016/j.jclepro.2018.01.206
5. Kaparaju P, Serrano M, Thomsen AB, Kongjan P, Angelidaki I (2009) Bioethanol, biohydrogen and biogas production from wheat straw in a biorefinery concept. Bioresour Technol 100:2562–2568. https://doi.org/10.1016/j.biortech.2008.11.011
6. Hyvärinen M, Ronkanen M, Kärki T (2019) The effect of the use of construction and demolition waste on the mechanical and moisture properties of a wood-plastic composite. Compos Struct 210:321–326. https://doi.org/10.1016/j.compstruct.2018.11.063
7. Ochi S (2008) Mechanical properties of kenaf fibers and kenaf/PLA composites. Mech Mater 40:446–452. https://doi.org/10.1016/j.mechmat.2007.10.006
8. Bernard M, Khalina A, Ali A, Janius R, Faizal M, Hasnah KS, Sanuddin AB (2011) The effect of processing parameters on the mechanical properties of kenaf fibre plastic composite. Mater Des 32:1039–1043. https://doi.org/10.1016/j.matdes.2010.07.014
9. Shibata S, Cao Y, Fukumoto I (2005) Press forming of short natural fiber-reinforced biodegradable resin: effects of fiber volume and length on flexural properties. Polym Test 24:1005–1011. https://doi.org/10.1016/j.polymertesting.2005.07.012
10. Yusoff RB, Takagi H, Nakagaito AN (2016) Tensile and flexural properties of polylactic acid-based hybrid green composites reinforced by kenaf, bamboo and coir fibers. Ind Crop Prod 94:562–573. https://doi.org/10.1016/j.indcrop.2016.09.017
11. Ali ME, Alabdulkarem A (2017) On thermal characteristics and microstructure of a new insulation material extracted from date palm trees surface fibers. Constr Build Mater 138:276–284. https://doi.org/10.1016/j.conbuildmat.2017.02.012
12. Okubo K, Fujii T, Yamamoto Y (2004) Development of bamboo-based polymer composites and their mechanical properties. Compos Part A Appl Sci Manuf 35:377–383. https://doi.org/10.1016/j.compositesa.2003.09.017
13. Deka H, Misra M, Mohanty A (2013) Renewable resource based " all green composites " from kenaf biofiber and poly (furfuryl alcohol) bioresin. Ind Crop Prod 41:94–101. https://doi.org/10.1016/j.indcrop.2012.03.037
14. de Farias JGG, Cavalcante RC, Canabarro BR, Viana HM, Scholz S, Simão RA (2017) Surface lignin removal on coir fibers by plasma treatment for improved adhesion in thermoplastic starch composites. Carbohydr Polym 165:429–436. https://doi.org/10.1016/j.carbpol.2017.02.042
15. Yousif BF, Shalwan A, Chin CW, Ming KC (2012) Flexural properties of treated and untreated kenaf/epoxy composites. Mater Des 40:378–385. https://doi.org/10.1016/j.matdes.2012.04.017
16. Yan L, Chouw N, Huang L, Kasal B (2016) Effect of alkali treatment on microstructure and mechanical properties of coir fibres, coir fibre reinforced-polymer composites and reinforced-cementitious composites. Constr Build Mater 112:168–182. https://doi.org/10.1016/j.conbuildmat.2016.02.182
17. Ilyas RA, Sapuan SM, Ishak MR, Zainudin ES (2018) Development and characterization of sugar palm nanocrystalline cellulose reinforced sugar palm starch bionanocomposites. Carbohydr Polym 202:186–202. https://doi.org/10.1016/j.carbpol.2018.09.002
18. Ilyas RA, Sapuan SM, Ishak MR (2018) Isolation and characterization of nanocrystalline cellulose from sugar palm fibres (Arenga pinnata). Carbohydr Polym 181:1038–1051. https://doi.org/10.1016/j.carbpol.2017.11.045

19. Yang X, Berthold F, Berglund LA (2019) High-density molded cellulose fibers and transparent biocomposites based on oriented holocellulose. ACS Appl Mater Interfaces 11:10310–10319. https://doi.org/10.1021/acsami.8b22134
20. Yang J, Ching Y, Chuah C (2019) Applications of lignocellulosic fibers and lignin in bioplastics: a review. Polymers (Basel) 11:751. https://doi.org/10.3390/polym11050751
21. Xu L, Meng L, Wu M et al (2014) Fully biodegradable composites of poly(butylene succinate)/enzymatic hydrolysis lignin: structure, thermal and mechanical properties. In: Lu F (ed) Lignin; structural analysis, Application in Biomaterials and Ecological Significance. Nova Science Publishers, Inc, New York, pp 112–126
22. Spiridon I, Tanase CE (2018) Design, characterization and preliminary biological evaluation of new lignin-PLA biocomposites. Int J Biol Macromol 114:855–863. https://doi.org/10.1016/j.ijbiomac.2018.03.140
23. Anugwom I, Lahtela V, Kallioinen M, Kärki T (2019) Lignin as a functional additive in a biocomposite: influence on mechanical properties of polylactic acid composites. Ind Crop Prod 140:111704. https://doi.org/10.1016/j.indcrop.2019.111704
24. Zadeh EM, O'Keefe SF, Kim YT (2018) Utilization of Lignin in Biopolymeric Packaging Films. ACS Omega 3:7388–7398. https://doi.org/10.1021/acsomega.7b01341
25. Luo S, Cao J, McDonald AG (2018) Cross-linking of technical lignin via esterification and thermally initiated free radical reaction. Ind Crop Prod 121:169–179. https://doi.org/10.1016/j.indcrop.2018.05.007
26. Engelmann G, Ganster J (2016) Lignin Reinforcement in Thermosets Composites. In: Lignin in Polymer Composites. Elsevier, pp 119–151. http://dx.doi.org/10.1016/B978-0-323-35565-0.00007-2
27. Kun D, Pukánszky B (2017) Polymer/lignin blends: Interactions, properties, applications. Eur Polym J 93:618–641. https://doi.org/10.1016/j.eurpolymj.2017.04.035
28. Rajesh Banu J, Kavitha S, Yukesh Kannah R, Poornima Devi T, Gunasekaran M, Kim SH, Kumar G (2019) A review on biopolymer production via lignin valorization. Bioresour Technol 290:121790. https://doi.org/10.1016/j.biortech.2019.121790
29. Panyakaew S, Fotios S (2011) New thermal insulation boards made from coconut husk and bagasse. Energy Build 43:1732–1739. https://doi.org/10.1016/j.enbuild.2011.03.015
30. Mobarak F, Fahmy Y, Augustin H (1982) Binderless lignocellulose composite from bagasse and mechanism of self-bonding. Holzforschung 36:131–136. https://doi.org/10.1515/hfsg.1982.36.3.131
31. Fahmy TYA, Mobarak F (2013) Advanced binderless board-like green nanocomposites from undebarked cotton stalks and mechanism of self-bonding. Cellulose 20:1453–1457. https://doi.org/10.1007/s10570-013-9911-9
32. Araújo Junior CP, Coaquira CAC, Mattos ALA, de Souza Filho MSM, Feitosa JPA, Morais JPS, de Freitas Rosa M (2018) Binderless fiberboards made from unripe coconut husks. Waste Biomass Valor 9:2245–2254. https://doi.org/10.1007/s12649-017-9979-9
33. Mancera C, El Mansouri NE, Ferrando F, Salvado J (2011) The suitability of steam exploded Vitis vinifera and alkaline lignin for the manufacture of fiberboard. BioResources 6:4439–4453
34. Quintana G, Velásquez J, Betancourt S, Gañán P (2009) Binderless fiberboard from steam exploded banana bunch. Ind Crop Prod 29:60–66. https://doi.org/10.1016/j.indcrop.2008.04.007
35. Reguant J, Montane D, Ferrando F, et al (1999) Binderless composites from pretreated residual softwood. 7–10. https://doi.org/10.1002/(SICI)1097-4628(19990919)73:12%3C2485::AID-APP17%3E3.0.CO;2-G
36. Suzuki S, Shintani H, Park SY, Saito K, Laemsak N, Okuma M, Iiyama K (1998) Preparation of binderless boards from steam exploded pulps of oil palm (Elaeis guneensis Jaxq.) fronds and structural characteristics of lignin and wall polysaccharides in steam exploded pulps to be discussed for self-bindings. Holzforschung 52:417–426. https://doi.org/10.1515/hfsg.1998.52.4.417
37. Miki T, Takeuchi K, Sugimoto H, Kanayama K (2007) Performance Study of compact wood powder material processing for improved impact characteristics aiming at substitute for plastics. J Mater Process Technol 193:422–427. https://doi.org/10.1016/j.jmatprotec.2007.04.078
38. Miki T, Takeuchi K, Sugimoto H, Kanayama K (2008) Material development from wood powder without adhesive by vapor steaming compaction process. J Mater Process Technol 199:396–401. https://doi.org/10.1016/j.jmatprotec.2007.08.010
39. Alharbi MAH, Hirai S, Tuan HA, Akioka S, Shoji W (2020) Effects of chemical composition, mild alkaline pretreatment and particle size on mechanical, thermal, and structural properties of binderless lignocellulosic biopolymers prepared by hot-pressing raw microfibrillated Phoenix dactylifera and Cocos nucifera. Polym Test 84:106384. https://doi.org/10.1016/j.polymertesting.2020.106384
40. Alharbi MAH, Hirai S, Tuan HA, Akioka S, Shoji W (2020) Dataset on mechanical, thermal and structural characterization of plant fiber-based biopolymers prepared by hot-pressing raw coconut coir, and milled powders of cotton, waste bagasse, wood, and bamboo. Data Br 30:105510. https://doi.org/10.1016/j.dib.2020.105510
41. Kaneko A, Tamada Y, Hirai S, Kuzuya T, Hashimoto T (2012) Characterization of a silk-resinified compact fabricated using a pulse-energizing sintering device. Macromol Mater Eng 297:272–278. https://doi.org/10.1002/mame.201100112
42. Tuan HA, Hirai S, Tamada Y, Akioka S (2019) Preparation of silk resins by hot pressing Bombyx mori and Eri silk powders. Mater Sci Eng C 97:431–437. https://doi.org/10.1016/j.msec.2018.12.060
43. Guo C, Li C, Vu HV, Hanna P, Lechtig A, Qiu Y, Mu X, Ling S, Nazarian A, Lin SJ, Kaplan DL (2020) Thermoplastic moulding of regenerated silk. Nat Mater 19:102–108. https://doi.org/10.1038/s41563-019-0560-8
44. Anh Tuan H, Hirai S, Inoue S, A. H. Mohammed A, Akioka S, Ngo Trinh T (2020) Fabrication of silk resin with high bending properties by hot-pressing and subsequent hot-rolling. Materials (Basel) 13:2716. https://doi.org/10.3390/ma13122716
45. Nakayama D, Wu F, Mohanty AK, Hirai S, Misra M (2018) Biodegradable composites developed from PBAT/PLA binary blends and silk powder: compatibilization and performance evaluation. ACS Omega 3:12412–12421. https://doi.org/10.1021/acsomega.8b00823
46. De Silva R, Wang X, Byrne N (2016) Development of a novel cellulose/duck feather composite fibre regenerated in ionic liquid. Carbohydr Polym 153:115–123. https://doi.org/10.1016/j.carbpol.2016.07.090
47. Hameed N, Guo Q (2010) Blend films of natural wool and cellulose prepared from an ionic liquid. Cellulose 17:803–813. https://doi.org/10.1007/s10570-010-9411-0
48. Shang S, Zhu L, Fan J (2011) Physical properties of silk fibroin/cellulose blend films regenerated from the hydrophilic ionic liquid. Carbohydr Polym 86:462–468. https://doi.org/10.1016/j.carbpol.2011.04.064
49. Kwak H, Shin M, Yun H, Lee K (2016) Preparation of Silk sericin/lignin blend beads for the removal of hexavalent chromium ions. Int J Mol Sci 17:1466. https://doi.org/10.3390/ijms17091466
50. Raschip IE, Hitruc GE, Vasile C, Popescu MC (2013) Effect of the lignin type on the morphology and thermal properties of the xanthan/lignin hydrogels. Int J Biol Macromol 54:230–237. https://doi.org/10.1016/j.ijbiomac.2012.12.036
51. Hubbe M, Pizzi AP, Zhang H (2018) Critical links governing performance of self-binding and natural binders for hot- pressed

reconstituted lignocellulosic board without added formaldehyde: a review Article. https://doi.org/10.15376/biores.13.1.Hubbe
52. Janković BŽ (2014) The pyrolysis behavior of lignins: contemporary kinetics overview. In: Lu F (ed) Lignin; structural analysis, Application in Biomaterials and Ecological Significance. Nova Science Publishers, New York, pp 330–351
53. JIS-K-7171 (2016) Plastics-determination of flexural properties. http://www.kikakurui. com/k7/K7171-2016-01.html
54. JIS-A-5905 (2014) Fiberboards. https://kikakurui.com/a5/A5905-2014-01.html.
55. Huang Y, Wang L, Chao Y, Nawawi DS, Akiyama T, Yokoyama T, Matsumoto Y (2012) Analysis of lignin aromatic structure in wood based on the IR spectrum. J Wood Chem Technol 32:294–303. https://doi.org/10.1080/02773813.2012.666316
56. Åkerholm M, Hinterstoisser B, Salmén L (2004) Characterization of the crystalline structure of cellulose using static and dynamic FT-IR spectroscopy. Carbohydr Res 339:569–578. https://doi.org/10.1016/j.carres.2003.11.012
57. Oh SY, Dong IY, Shin Y et al (2005) Crystalline structure analysis of cellulose treated with sodium hydroxide and carbon dioxide by means of X-ray diffraction and FTIR spectroscopy. Carbohydr Res 340:2376–2391. https://doi.org/10.1016/j.carres.2005.08.007
58. Poletto M, Ornaghi Júnior HL, Zattera AJ (2014) Native cellulose: structure, characterization and thermal properties. Materials (Basel) 7:6105–6119. https://doi.org/10.3390/ma7096105
59. Faix O (1992) Fourier transform infrared spectroscopy. Springer Ser Wood Sci 14:83–109. https://doi.org/10.1007/978-3-642-74065-7_7
60. Werner K, Pommer L, Broström M (2014) Thermal decomposition of hemicelluloses. J Anal Appl Pyrolysis 110:130–137. https://doi.org/10.1016/j.jaap.2014.08.013
61. Hu X, Kaplan D, Cebe P (2006) Determining beta-sheet crystallinity in fibrous proteins by thermal analysis and infrared spectroscopy. Macromolecules 39:6161–6170. https://doi.org/10.1021/ma0610109
62. Kong J, Yu S (2007) Fourier transform infrared spectroscopic analysis of protein secondary structures. Acta Biochim Biophys Sin Shanghai 39:549–559. https://doi.org/10.1111/j.1745-7270.2007.00320.x
63. Heinze T, El Seoud OA, Koschella A (2018) Cellulose activation and dissolution. Springer Series on Polymer and Composite Materials, Cham, pp 173–257
64. Batiancela MA, Acda MN, Cabangon RJ (2014) Particleboard from waste tea leaves and wood particles. J Compos Mater 48:911–916. https://doi.org/10.1177/0021998313480196
65. Lamaming J, Sulaiman O, Sugimoto T et al (2013) Influence of chemical components of oil palm on properties of binderless particleboard. BioResources 8:3358–3371. https://doi.org/10.15376/biores.8.3.3358-3371
66. Hashim R, Nadhari WNAW, Sulaiman O, Kawamura F, Hiziroglu S, Sato M, Sugimoto T, Seng TG, Tanaka R (2011) Characterization of raw materials and manufactured binderless particleboard from oil palm biomass. Mater Des 32:246–254. https://doi.org/10.1016/j.matdes.2010.05.059
67. Arévalo R, Peijs T (2016) Binderless all-cellulose fibreboard from microfibrillated lignocellulosic natural fibres. Compos Part A Appl Sci Manuf 83:38–46. https://doi.org/10.1016/j.compositesa.2015.11.027
68. Fang Z, Weisenberger MC, Meier MS (2020) Utilization of lignin-derived small molecules: epoxy polymers from lignin oxidation products. ACS Appl Bio Mater 3:881–890. https://doi.org/10.1021/acsabm.9b00954
69. Jakab E, Faix O, Till F, Székely T (1995) Thermogravimetry/mass spectrometry study of six lignins within the scope of an international round robin test. J Anal Appl Pyrolysis 35:167–179. https://doi.org/10.1016/0165-2370(95)00907-7
70. Monteil-Rivera F, Phuong M, Ye M, Halasz A, Hawari J (2013) Isolation and characterization of herbaceous lignins for applications in biomaterials. Ind Crop Prod 41:356–364. https://doi.org/10.1016/j.indcrop.2012.04.049
71. Kim JY, Shin EJ, Eom IY, Won K, Kim YH, Choi D, Choi IG, Choi JW (2011) Structural features of lignin macromolecules extracted with ionic liquid from poplar wood. Bioresour Technol 102:9020–9025. https://doi.org/10.1016/j.biortech.2011.07.081
72. Kabir AS, Yuan Z, Kuboki T, Xu C(C) (2018) De-polymerization of industrial lignins to improve the thermo-oxidative stability of polyolefins. Ind Crop Prod 120:238–249. https://doi.org/10.1016/j.indcrop.2018.04.072
73. Reis JS, Araujo RO, Lima VMR, Queiroz LS, da Costa CEF, Pardauil JJR, Chaar JS, Rocha Filho GN, de Souza LKC (2019) Combustion properties of potential Amazon biomass waste for use as fuel. J Therm Anal Calorim 138:3535–3539. https://doi.org/10.1007/s10973-019-08457-5
74. Fan M, Dai D, Huang B (2012) Fourier transform infrared spectroscopy for natural fibres. Fourier Transform - Mater Anal 45–68. https://doi.org/10.5772/2659
75. Ha SW, Tonelli AE, Hudson SM (2005) Structural studies of Bombyx mori silk fibroin during regeneration from solutions and wet fiber spinning. Biomacromolecules 6:1722–1731. https://doi.org/10.1021/bm050010y
76. Riaz T, Zeeshan R, Zarif F, Ilyas K, Muhammad N, Safi SZ, Rahim A, Rizvi SAA, Rehman IU (2018) FTIR analysis of natural and synthetic collagen. Appl Spectrosc Rev 53:703–746. https://doi.org/10.1080/05704928.2018.1426595
77. Oliviero M, Verdolotti L, Di Maio E et al (2011) Effect of supramolecular structures on thermoplastic zein–lignin bionanocomposites. J Agric Food Chem 59:10062–10070. https://doi.org/10.1021/jf201728p
78. Athamneh AI, Griffin M, Whaley M, Barone JR (2008) Conformational changes and molecular mobility in plasticized proteins. Biomacromolecules 9:3181–3187. https://doi.org/10.1021/bm800759g